

Environmental Effects on Non-oxide Ceramics

Nathan S. Jacobson and Elizabeth J. Opila

NASA Lewis Research Center

Cleveland, OH 44135

I. Introduction

Non-oxide ceramics such as silicon carbide (SiC) and silicon nitride (Si_3N_4) are promising materials for a wide range of high temperature applications. These include such diverse applications as components for heat engines, high temperature electronics, and re-entry shields for space vehicles. Table I lists a number of selected applications. Most of the emphasis here will be on SiC and Si_3N_4 . Where appropriate, other non-oxide materials such as aluminum nitride (AIN) and boron nitride (BN) will be discussed. Proposed materials include both monolithic ceramics and composites. Composites are treated in more detail elsewhere in this volume, however, many of the oxidation/corrosion reactions discussed here can be extended to composites. In application these materials will be exposed to a wide variety of environments. Table I also lists reactive components of these environments.

* Resident Research Associate, Cleveland State University, Cleveland, OH 44115

It is well-known that SiC and Si_3N_4 retain their strength to high temperatures. Thus these materials have been proposed for a variety of hot-gas-path components in combustion applications. These include heat exchanger tubes, combustor liners, and porous filters for coal combustion products. All combustion gases contain CO_2 , CO, H_2 , H_2O , O_2 , and N_2 . The exact gas composition is dependent on the fuel to air ratio or equivalence ratio. (Equivalence ratio (EQ) is a fuel-to-air ratio, with total hydrocarbon content normalized to the amount of O_2 and defined by EQ=1 for complete combustion to CO_2 and H_2O). Figure 1 is a plot of equilibrium gas composition vs. equivalence ratio. Note that as a general rule, all combustion atmospheres are about 10% water vapor and 10% CO_2 . The amounts of CO, H_2 , and O_2 are highly dependent on equivalence ratio.

Other proposed applications for SiC include high temperature semi-conductors and for AlN include electronic substrates. In these situations, high temperature oxidation behavior is a prime issue. Re-entry shields have long been a useful application of ceramic materials—here the environment is a complex mixture of atoms and molecules. Finally a growing area is the application of ceramics as pump components and ball bearings. The environment depends on the fluid of interest, but is generally high temperature/high pressure water.

In this chapter we will discuss the interaction of non-oxide ceramics with some representative environments. We begin with pure oxidation which is important for nearly all the applications and then proceed to the more system-specific environments such as molten salts and high pressure water.

II. High Temperature Oxidation

Figure 2 summarizes oxidation behavior for a range of non-oxide ceramics (14). These data are presented in terms of recession in one hundred hours. Clearly long-term operation requires very low recession. The key oxidation reactions can be summarized as follows:

1. Silica formers— SiC , Si_3N_4 , MoSi_2



The oxidation of SiC and Si_3N_4 is described in detail in the following section.

2. Alumina formers—primarily alloys, but also AlN



The underline indicates aluminum is at less than unity activity, as would be found in an alloy.



The oxidation of AlN is discussed more fully in the following section.

3. Borides



4. Carbides



5. Nitrides



or



Most of these materials oxidize according to a parabolic rate law, but some oxidize according to linear kinetics. Hence Figure 2 gives oxidation kinetics in terms of recession to account for both kinetic laws. The reader is referred to (14) and references contained therein for more details on the kinetics of these reactions.

The important point from Figure 2 is that only materials which form protective silica or alumina films are useful for long times in oxidizing environments. Most of the borides, carbides, and nitrides do not form protective metal oxide scales. Hence the focus of this chapter will be on silica forming ceramics, SiC and Si_3N_4 .

and the alumina forming ceramic, AlN. We shall also include a brief discussion of BN, which is an important material in many areas of technology.

II.A. Oxidation of SiC and Si_3N_4

II.A.1. Oxygen Transport in Silica

The low oxidation rates of silica-forming ceramics are due to remarkably low oxygen transport rates in silica. Thus we begin with a brief discussion of oxygen transport in silica. Amorphous silica, found for short-time oxidation or in very clean systems, consists of a random network of Si-O tetrahedra as shown schematically in Figure 3a (15). Cristobalite, the crystalline form of silica most often observed after long-term oxidation or oxidation in less clean environments, is composed of the same Si-O tetrahedra but arranged in an orderly structure as shown in Figure 3b.

Oxygen transport through these structures occurs by two different mechanisms. First, molecular oxygen can move through the interstices between the tetrahedra by a permeation mechanism. Alternatively, ionic oxygen can move from network site to network site by a bond breaking exchange mechanism. The permeation mechanism requires less activation energy since bond breaking is not required. Permeation through cristobalite is expected to be slower than through

amorphous silica since the regular structure is restricted to six member oxygen rings whereas the irregular structure found in amorphous silica allows for seven and eight member rings (15).

Permeation rates of molecular oxygen in amorphous silica have been determined (16), however, the corresponding rates in cristobalite have not been measured. The measurements are difficult since bulk cristobalite is not available and must be nucleated and characterized at temperature. In addition, the presence of short circuit transport paths along cristobalite grain boundaries and cracks formed from the β to α cristobalite phase transformation upon cooling make the measurement of intrinsic oxygen transport rates in cristobalite impossible.

II.A.2. Oxidation of silica forming ceramics—Experimental Techniques

Oxidation kinetics for these materials are determined by measuring either weight changes using a sensitive thermogravimetric balance as shown in Figure 4 or oxide thickness changes using optical techniques. An example of weight change versus time for SiC oxidation in dry oxygen is shown in Figure 5. Since the oxidation rate is controlled by diffusion of oxygen through the silica scale, the weight change decreases with time according to a parabolic law and is described by the parabolic rate constant, k_p . Accurate determinations of oxidation kinetics are more difficult for silica forming materials than for other metal-oxide forming

materials because silica grows at such a slow rate, and because silica growth kinetics are affected by even small amounts of impurities in the sample or oxidation environment (17). A comparison of the parabolic oxidation rates for silicon, SiC, and Si_3N_4 as a function of temperature is shown in Figure 6. Similarities and differences in the oxidation kinetics of these materials are discussed in the following sections.

It is instructive to begin with the relatively simple case of silicon oxidation. We will then focus on very pure SiC and Si_3N_4 in order to understand the fundamental oxidation behavior of these materials. These pure materials are also important in microelectronic applications.

II.A.3. Oxidation of Silicon

Silicon oxidation has been studied in great detail due to its application in microelectronic devices. The model of Deal and Grove (18) has been used to successfully describe silicon oxidation behavior at all but the shortest times. This model considers two possible rate limiting steps for the oxidation of silicon. First the reaction of oxygen with silicon according to a linear rate law controls the oxidation rate at short times or for thin scales. Second, transport of oxygen through the growing silica scale controls the oxidation rate according to a parabolic rate law for long times and for thick scales. These two rate laws are combined into a single expression that is valid for all times:

$$\frac{x_o}{A/2} = \frac{T}{M} \frac{t+\tau}{N A^2 / 4B}^{1/2} - 1 \quad (8)$$

where x_o is the oxide thickness, t is time, τ is the offset time which corrects for the presence of an initial oxide layer, B is the parabolic rate constant and B/A is the linear rate constant. At short times this expression simplifies to the linear rate law $x_o = (t+\tau)B/A$ while at long times the expression simplifies to the parabolic law $x_o^2 = Bt$. For long-term applications of silica forming materials, the parabolic law usually describes the oxidation kinetics adequately.

Deal and Grove have derived the parabolic rate constant in terms of the properties of silica, i.e.:

$$B = 2D_{eff}C^*/N \quad (9)$$

and

$$C^* = kP^n \quad (10)$$

where D_{eff} is the effective diffusivity of oxidant in silica, C^* is the equilibrium concentration of oxidant in the oxide, N is the number of oxidant molecules incorporated into a unit volume of the oxide layer, P is the oxidant pressure, n is a power law exponent, and k is a constant. The parabolic rate constant was found to vary linearly with the oxidant pressure for both oxygen and water vapor, i.e., $n=1$, indicating that the oxidant did not dissociate and molecular permeation through the silica is the rate limiting step for oxidation in the parabolic regime.

II.A.4. Oxidation of SiC

The oxidation of SiC is similar to the oxidation of silicon since a silica scale forms in both cases. In this case, however, the gases generated, as shown in the following oxidation reactions, will cause some differences:



The linear reaction rate is different since the oxidation of C to CO(g) or CO₂(g) occurs in addition to the oxidation of Si. The parabolic oxidation rate could be different if the outward transport of CO or CO₂, rather than the inward transport of oxygen, limited the oxidation rate. It has been shown that the oxidation rates of SiC are about a factor of two slower than silicon (19-21) due to the extra consumption of oxygen in the reaction with C, as predicted (22). In addition, the activation energy for oxidation (20) is nearly identical to that of silicon (18) (see Figure 6) and the permeation of molecular oxygen through silica (16). Finally, the oxidation rate of SiC is found to depend on the oxygen partial pressure (23). Therefore, it is generally agreed that oxygen transport inward is the rate limiting step for parabolic oxidation of SiC. This issue has been discussed more fully in other references (24, 25).

The dependence of the parabolic rate constant on the oxygen partial pressure, given by the power law exponent, n, in Equation 10 above, gives information about the type of oxygen transport occurring in the silica. For n=1 molecular permeation of oxygen occurs. For n<1, some dissociation of oxygen into a

charged species occurs and network diffusion of oxygen by a bond breaking process is likely. Zheng et al. (23) have determined the power law exponent for the oxidation of SiC to vary between 0.6 and 0.3 at temperatures from 1200 to 1500°C. This implies that some combination of permeation and network diffusion limits the oxygen transport through the silica scale grown on SiC, with network diffusion increasing with temperature. This is confirmed by ^{18}O tracer diffusion studies which show isotope exchange with network oxygen becomes increasingly important as the temperature is increased (26). However, the similar activation energies for molecular oxygen permeation of silica (16) and for oxidation of SiC up to temperatures of 1500°C (20) indicates that oxygen transport is dominated by the permeation mechanism.

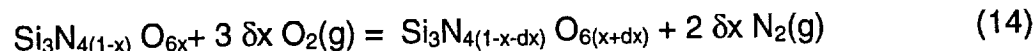
The effect of crystallization of silica on SiC oxidation is a complex topic. Some investigators have used crystallization to explain observed rate changes and/or activation energy changes. However, current evidence indicates that many of these deviations in rate law and activation energies can be explained by impurities in either the environment or the SiC (17, 20, 27, 28). Ogbuji (29) has shown that silica scales *fully* crystallized during argon anneals at 1300°C do result in slower oxidation rates by about a factor of 30, but that fully crystalline scales are not found in actual practice since amorphous silica is continually formed during the course of SiC oxidation.

II.A.5. Oxidation of Si_3N_4

Like SiC, the oxidation of Si_3N_4 results in the formation of a silica layer and the generation of gaseous products according to the following simplified reaction:



An additional complication, however, is the formation of a suboxide layer of amorphous silicon oxynitride of variable stoichiometry (30, 31). The oxidation reaction can be written as (32):



for x varying between 0 and 1. Measurements of the oxidation kinetics of Si_3N_4 have shown they are parabolic, but significantly slower than oxidation of both silicon (33) and SiC (20) to temperatures of 1500°C. Pure Si_3N_4 is the slowest oxidizing material known today. The higher activation energy for Si_3N_4 reflects the additional energy required in the breaking of bonds for the nitrogen-oxygen substitution reaction. The oxidation rates were found to be dependent on the oxygen partial pressure, but independent of the nitrogen partial pressure (33). In this case, the oxidation reaction is limited by oxygen transport and reaction in the oxynitride layer (32) rather than by oxygen transport in silica.

II.A.6. Oxidation of Additive-Containing Materials

The above discussions have considered only very pure materials. SiC and Si_3N_4 materials used for structural applications often contain additives to aid sintering. These additives affect long-term oxidation behavior. First, additives can diffuse into the silica scale during oxidation (34-38). Impurities present in silica increase oxygen transport rates by modification of the silica network structure and thereby increase oxidation rates of the silica-forming material (39). Second, additives such as Y_2O_3 , La_2O_3 , MgO , and CeO_2 present in significant amounts (4-10%) will diffuse to the silica surface and form discrete particles of silicates often of the $\text{M}_2\text{Si}_2\text{O}_7$ phase where M=Y, La, Ce. In these cases, the oxidation kinetics are still parabolic to times as long as 1000h (D.S. Fox, personal communication, 1997), but limited by the outward diffusion of metal cations to the matrix/oxide interface (34,35). In addition, for silicon nitride ceramics, the presence of impurities (40) and additives (41) prevent the formation of the silicon oxynitride inner layer, thus, oxidation rates of Si_3N_4 in practical applications are never as low as those found for pure CVD Si_3N_4 . As additive levels and impurities increase further, the oxidation kinetics often do not follow simple parabolic rate laws. These more complex oxidation kinetics have been modeled in various ways (42,43). Finally, for systems containing large amounts of additives, >10%, at intermediate temperatures 1000-1200°C, reactions to form silicates occur in the grain boundaries with a volume expansion large enough to cause disintegration of the ceramic (44).

II.A.7. Thermal Cycling Effects

Long-term applications of structural ceramics, such as heat engines, require thermal cycling. Thermal cycling is a concern for several reasons. First, upon cooling, cristobalite undergoes the β to α phase transformation with an accompanying 3% volume contraction (45). This volume change causes cracks to form in cristobalite upon cooling. Second, the thermal mismatch between SiC or Si_3N_4 and cristobalite, shown in Figure 7, results in tensile stresses in the oxide layer upon cooling. Cracks in the oxide may then form. However, cyclic oxidation tests at 1300°C in 5-hour cycles for 1000 hours have shown little deleterious effects on the oxidation kinetics when measured by weight change (46), as shown in Figure 8. One possible explanation is that upon reheating, stress is relieved and the cracks heal. Note that the tensile stresses formed in these ceramic/oxide systems contrast with those in superalloy/oxide systems where compressive stresses form in the scale on cooling and oxide spallation is typically observed.

II.B. Oxidation of other non-oxide Ceramics

BN is a useful crucible material in a vacuum or inert atmosphere. However, in oxygen it readily forms a liquid B_2O_3 scale which is not protective (47). Furthermore this B_2O_3 scale readily reacts with water vapor and forms stable volatile H-B-O(g) species, such as $HBO_2(g)$, $H_3BO_3(g)$, and $H_3B_3O_6(g)$. These species have strongly negative free energies of formation and form even with ppm levels of water vapor. A similar situation exists with TiB_2 , which is an attractive structural material due to its high strength (48).

AlN is currently a candidate for electronic substrates due to its high thermal conductivity (9). As an alumina former, it is expected to exhibit slow oxidation kinetics. However it appears to oxidize quite rapidly above about 1000°C, with rates quite dependent on grain size, porosity, the presence of second phases, and impurity content (49). In many instances, linear kinetics have been reported, in contrast to alumina formation on metal alloys (50). In addition, it is well established that water vapor in the oxidizing stream leads to extensive attack (51). The reasons for this extensive alumina formation in dry and wet oxygen are not clear. Clearly, nitrogen must escape through the alumina scale, which may lead to micropore formation. It has been suggested that the injection of N^{3-} leads to excess vacancy formation in the alumina and more rapid diffusion rates (52). In addition, the CTE mismatch between AlN and Al_2O_3 may lead to scale cracking (53).

III. Complex Environments

In most applications, ceramic materials are subjected to more aggressive environments than high temperature oxygen alone. These are outlined in Table I. As in the case of pure oxidation, most of the available data on interactions of non-oxide ceramics in complex gas mixtures are for SiC and Si_3N_4 .

III.A. Water Vapor

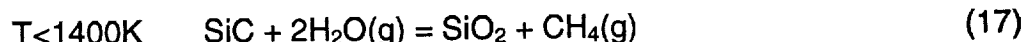
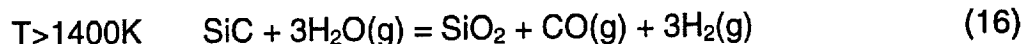
There is general agreement that water vapor enhances the oxidation rate of silicon, SiC and Si_3N_4 . There is a large amount of disagreement as to the magnitude of this effect for SiC and Si_3N_4 . This disagreement arises in part from the complex effects water vapor has on the growing silica scale. These effects include enhanced impurity transport to the silica scale in water vapor containing atmospheres, enhanced solubility of water in the silica scale, alterations in the silica scale viscosity and structure, and finally, formation of volatile silicon hydroxide and oxyhydroxide species. Each one of these topics will be discussed separately below. Again, references to the oxidation behavior of silicon in water vapor are made for comparison.

Oxidation of silicon by water vapor occurs by the following reaction:

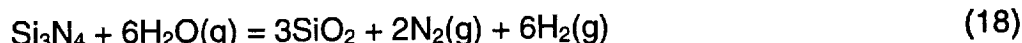


The enhanced growth rates of SiO_2 by this reaction, relative to dry oxygen, has commercial application in the more rapid fabrication of microelectronic devices.

Oxidation of SiC by water vapor occurs by the reactions (54):



and for Si_3N_4 by the following reaction:



Note that in each case the solid product SiO_2 is formed with the generation of additional gaseous products.

III.A.1. Impurity Transport

Impurities normally found in water vapor-containing environment form M-OH(g) species, where M is the impurity element such as Na, K, Fe, etc. Since M-OH(g) species are so thermodynamically stable, the quantity of impurities transported to a silica scale forming on SiC or Si_3N_4 in a water-vapor containing environment is increased. This increased contamination of the silica scale results in faster transport rates of oxidant through the scale, and thus increased oxidation rates of SiC or Si_3N_4 . This effect has been identified for both Na- (55) and K-contamination (56) during the oxidation of SiC .

III.A.2. Enhanced solubility of water in the silica scale

Deal and Grove (18) have shown that the parabolic oxidation rate of silicon in water vapor is increased by about an order of magnitude over the rate found in dry oxygen. This is explained by examination of Equation 9. While the diffusivity of water vapor in silica is almost two orders of magnitude slower than molecular oxygen, the solubility of water is nearly three orders of magnitude larger than oxygen. The net result is that parabolic oxidation rates of silicon in water vapor are more than one order of magnitude larger than those observed in dry oxygen. This explanation is directly applicable to the discussion for SiC and Si_3N_4 since silica is the oxidation product for these materials. This enhancement in parabolic oxidation rate constants has been observed for SiC (55,57) and in some cases for Si_3N_4 (58).

Deal and Grove (18) have also demonstrated that the parabolic oxidation rate has a power law dependence on the water vapor partial pressure, with the power law exponent, n (Equation 10), equal to one, indicating that molecular water diffusion is the rate controlling step in the oxidation of silicon. Power law exponents for the oxidation of SiC of 0.67 (59) and of about 0.5 (54) have been obtained. This indicates dissociation of water into a singly charged species is probable. The discrepancy between the findings for silicon and SiC is unexpected since the transport properties of silica should be independent of the substrate material. A complex relationship between parabolic rate constant and

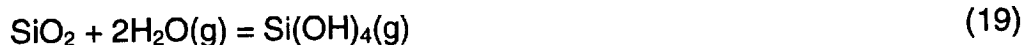
water vapor partial pressure has been observed for Si_3N_4 (58), but this may be explained by silica volatility, as described in section III.A.4.

III.A.3. Alterations in the structure of silica

It has been shown that the viscosity of amorphous silica decreases as the hydroxyl content increases (60). Hydroxyl groups are effective in breaking Si-O-Si bonds in amorphous silica. It is suggested that the resulting silica allows the more rapid permeation of molecular oxygen (57). The reduced viscosity of amorphous silica in conjunction with increased amounts of gaseous products results in the formation of bubbles in the scale formed on SiC (54) as shown in Figure 9. These bubbles, in turn, create shorter transport paths for oxidant to the SiC/ SiO_2 interface by decreasing the effective oxide thickness, thereby increasing the oxidation rate. In contrast, bubbles are not observed in the scales formed on SiC in dry oxygen or on silicon in wet oxygen.

III.A.4. Silica scale volatility

Water vapor reacts with the silica scale formed on SiC and Si_3N_4 to form volatile hydroxide and oxyhydroxide species by the following reactions:



These volatile silicon hydroxides and oxyhydroxides have been identified experimentally using the transpiration technique (61) as well as mass spectrometry (62). The reaction of water vapor with SiC or Si₃N₄ involves the oxidation reaction (Equations 16-18) and the simultaneous linear volatilization reaction (Equations 19-20) resulting in overall paralinear kinetics (63). Paralinear kinetics, as measured by weight change, are shown in Figure 10. At long times, the weight change and recession can be approximated by the linear volatilization rate alone. At this time a steady state is achieved, the silica scale is consumed at the same rate it is formed leaving a constant oxide thickness. The volatilization rate of silica is controlled by transport of the volatile species through a gaseous boundary layer (63). This boundary layer controlled volatility rate can be expressed in terms of the application conditions such as gas velocity, total pressure, and water vapor partial pressure. For Si(OH)₄(g) formation, the volatility rate has the following dependences:

$$k_i \propto \frac{v^{1/2} P(H_2O)^2}{P_{\text{total}}^{1/2}} \quad (21)$$

where k_i is the linear volatility rate, v is the gas velocity and P is pressure. Thus, in high pressure and high velocity applications, such as a gas turbine engine, the recession of a SiC or Si₃N₄ component by the volatility mechanism can be significant.

In summary, water vapor has deleterious effects on the durability of silica formers through a number of different mechanisms: Increased transport of impurities to the oxide surface, increased oxide formation rates due to impurity

effects, enhanced solubility of water vapor, short circuit paths for oxidant transport, increased permeability of the oxidant, and finally consumption of the silica scale and component recession due to silica volatility.

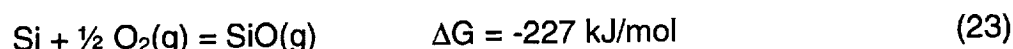
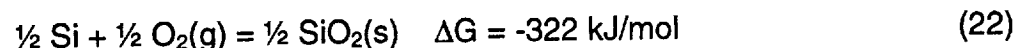
III.B. Carbon Dioxide

Although CO₂ is a major component of combustion gases (Figure 1), there are only a few limited oxidation studies of SiC in CO₂ (64-67). It has been found that the oxidation rates of SiC in CO₂ are less than those in oxygen. Because the oxide growth rates are so low it is difficult to determine whether the kinetics are linear, parabolic, or more complex. The oxidation weight gain for SiC in CO₂ is shown compared to that observed in oxygen and a 50% water vapor/oxygen mixture in Figure 11 (67). Thus, in a complex combustion environment, the effects of CO₂ as an oxidant are negligible.

III.C. Effects of low P(O₂), Reducing Gases, H₂S, Cl₂

III.C.1. SiO(g) Formation

A unique, but very important issue with silica formers is the highly stable volatile sub-oxide, SiO(g). Consider the free energy of formation at 1500 K:



Note these equations are normalized to one mole of oxygen atoms. The free energies of formations are close, indicating SiO(g) can readily form.

There are two conditions which lead to SiO(g) formation (68): active oxidation and oxidation in mixed oxidizing/reducing gases. In the active oxidation case, the partial pressure of oxygen is too low to form a stable SiO₂ film, but sufficient to form SiO(g). This can occur in certain heat treating environments (69). Let us begin with a bare SiC surface. As the partial pressure of oxygen is increased, SiO(g) will form in increasing quantities. Then SiO(g) formation will stop and a stable SiO₂ film will form. This is the active-to-passive transition. Wagner has derived this for pure silicon (70). His results can be easily extended to SiC and Si₃N₄ (71). The active-to- passive transition occurs when sufficient SiO(g), via Equation 23, is generated to satisfy the SiC/SiO₂ condition for equilibrium. There is some controversy about the exact equilibrium condition, but reasonable agreement with measurements is obtained from the following equilibria:



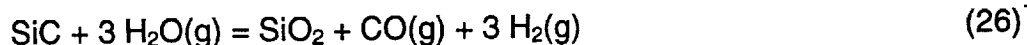
The transition P(O₂) for active-to-passive oxidation is calculated based on equilibrium conditions and diffusion through the gas boundary layer to the sample. Calculated and measured active-to-passive transitions (72-74) are shown in Figure 12.

Now consider the case of passive-to-active transition. Beginning with a stable SiO_2 film on SiC, as the partial pressure of oxygen is lowered the film will become unstable and SiO_2 will react to form SiO(g) . The transition pressure is calculated from the decomposition of the protective SiO_2 film (70):



The calculated passive-to-active line is shown in Figure 12—note it is several orders of magnitude lower than the active-to-passive transition.

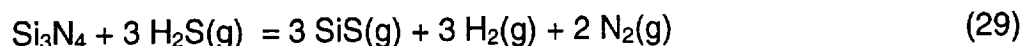
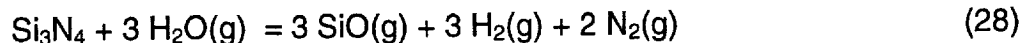
A second route to SiO(g) formation occurs in a mixture of oxidizing and reducing gases (68). These can be present in a fuel-rich combustion situation with appreciable amounts of CO_2 , CO , H_2O and H_2 . It has also been observed in laboratory experiments with CO/CO_2 (73) and $\text{H}_2/\text{H}_2\text{O}$ (72). Thus a sequence of reactions might be:



This leads to paralinear kinetics—simultaneous oxide growth and linear reduction kinetics.

III.C.2 Effects of H_2S and Cl_2

Hydrogen sulfide is found in coal gasifiers and various other petrochemical environments (5). At low oxygen potentials, when SiO_2 does not form, both SiO(g) and SiS(g) may form:



These reactions can lead to material consumption (5), however when the oxygen potential is high enough to form SiO_2 , the corrosion rate drops substantially.

Chlorine, which may be found in certain chemical process environments, also leads to volatile products (75). In the case of SiC, reaction occurs with the silicon, leading to formation of various silicon chlorides with residual carbon. As the oxygen potential is increased, attack becomes less severe (75).

Current interest focuses on chlorine as HCl in waste incineration applications (76). Here the situation is quite complex involving not only HCl, but also a range of deposits.

III.D. Oxidation in the Presence of Impurities and Deposits

III.D.1. Low Levels of Na and K

Small amounts of impurities have several possible effects on the structure and thus the transport properties of silica. First, impurities can nucleate the formation of cristobalite at temperatures and times where amorphous silica would be expected. Second, impurities can modify the silica network as shown in Figure 3c. Breaking up the network tends to increase the oxygen transport rate through silica. Small amounts of alkali metals act as network modifiers and can increase oxidation rates an order of magnitude (56, 77, 78).

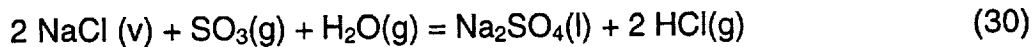
III.D.2. Na₂SO₄ Deposits

As impurity levels increase, actual deposits may form. The chemistry of these depends on application, as shown in Table I. Corrosive deposits have long been known to be an important issue for metals and alloys in various high temperature applications (79). Here we shall focus on sodium sulfate deposits on silica. Many of the general principles described for this system apply to the other cases.

It is difficult to simulate the effect of an actual deposit. Simple laboratory experiments involve a one-time deposition of a salt on a test coupon, followed by

a heat treatment. This type of experiment has the advantage of precise control of experimental variables such as temperature and gas composition. However, the actual situation involves a continuous deposition process. This can be done in a laboratory furnace. However this can be accomplished more effectively by seeding a flame in a burner rig, as illustrated in Figure 13. Figure 14 is a comparison of SiC treated in a burner without salt and with a flame seeded with NaCl. Note the extensive corrosion in the latter case.

The formation of Na₂SO₄ occurs when ingested NaCl reacts with sulfur impurities in the fuel (80, 81):



The source of NaCl depends on the application—it may be from a marine environment in the case of a heat engine, or from the process chemicals in the case of an industrial furnace. Under the appropriate conditions, Na₂SO₄ forms as a condensed phase, depositing on parts. Figure 15 shows the calculated dew points for Na₂SO₄ deposition (81). The rates of deposition are also critical and have been treated in detail (82).

The most useful interpretation of this process is with the acid/base theory of molten salts. Na₂SO₄ decomposes to Na₂O, which is the key reactant:

salt solution models (84) and leads to Mg and Ca silicates. Impure fuels lead to vanadate deposits. V_2O_5 is an acidic molten salt and thus does not react with SiO_2 . However it is reported to accelerate Si_3N_4 oxidation, possibly due to the solubility of SiO_2 in V_2O_5 which may be further enhanced by the presence of a Y_2O_3 in Si_3N_4 (85).

A more complex case is that of a molten slag, which may contain up to ten different oxides. Here it more difficult to define basicity, however a useful index has been the weight percent ratio of basic to acid oxides (86). These are the basic and acidic oxides encountered:

Basic Oxides: Na_2O , K_2O , MgO , CaO , Fe_2O_3

Acidic Oxides: SiO_2 , Al_2O_3 , TiO_2

As in the Na_2SO_4 case, the basic slag tends to cause more rapid material degradation than the acidic slag. Under some conditions, metal silicides may form with a basic coal slag (4).

III.E. High Temperature Effects

Silica melts at 1723°C. Transport rates are very high in a liquid scale and rapid oxidation occurs, as shown in Figure 17. Some of the bubbles in this sample are from escape of CO(g), but some are also from the interaction of SiC and SiO₂ at high temperatures:

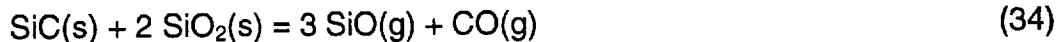
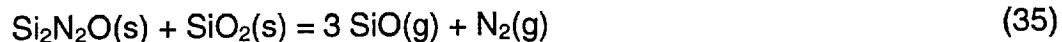


Figure 18a is a plot of total pressures generated by this reaction (87). Note that for carbon saturated SiC the pressures are much higher, leading to a lower upper use temperature. An analogous situation exists for Si₃N₄, but based on the Si₂N₂O interaction with SiO₂:



The total pressure is shown in Figure 18b.

IV. Refractory Oxide Coatings

One possible solution to the preceding issues of volatility and molten salt corrosion is the use of refractory oxide coatings on SiC and Si₃N₄. Refractory oxides are generally more chemically inert and this approach offers the possibility of combining the benefits of both materials. Table II lists some coefficients of thermal expansion (CTEs) for SiC, Si₃N₄, and refractory oxides. There is a good match between SiC and mullite. Mullite coatings on SiC were

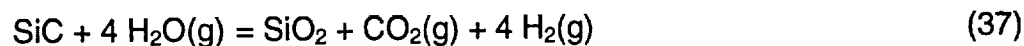
first developed at Solar Turbines (San Diego, CA) and further developed at NASA Lewis (88, 89). The critical processing issues are surface roughening of the SiC for adherence and application of a fully crystalline mullite coating. A mullite coating on a SiC coupon is shown in Figure 19. There are clear advantages with mullite coatings in Na₂O-induced corrosion due to formation of high melting sodium-alumino-silicates, as opposed to lower melting sodium silicates. However the chemical activity of silica in mullite is only about 0.4, so reactions which volatilize SiO₂ can still occur readily.

It may be possible to apply other refractory oxides to SiC. As Table II shows, the problem of CTEs must be considered. One approach is graded coatings from SiC to a refractory oxide such as alumina or zirconia.

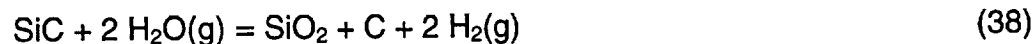
V. Hydrothermal Corrosion of SiC and Si₃N₄

Hydrothermal corrosion involves the attack by water at high temperatures and high pressures. Typical conditions are shown in Table I. These conditions are often near the critical point of water. Table I also shows some potential applications where these environments may be encountered. Another promising application of SiC and Si₃N₄ is a vessel for oxidation of waste materials to form safe products using super-critical water (90).

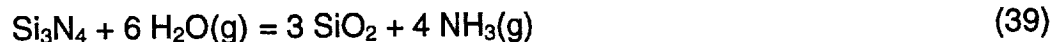
The hydrothermal corrosion of SiC may form silica by the following reactions (91, 92):



Given nearly equal amounts of SiC and water vapor at high temperatures, free carbon can form (92, 93):



This provides a method for synthesis of carbon films. However, in most applications there is excess water and SiO₂ is formed as a protective film. The hydrothermal corrosion of Si₃N₄ is similar and occurs by:



At temperatures above 430°C, NH₃(g) decomposes to N₂(g) and H₂(g).

In both cases, the silica is eventually dissolved by the high pressure water as:



In the case of Si_3N_4 , this leads to attack of the grain boundary phases and dislodging of the grains (94). Methodical studies have been done on the effect of additives in Si_3N_4 on its hydrothermal corrosion behavior (13, 94). The morphology of attack has been correlated with the type of additive and its resistance to hydrothermal attack.

Ceramics which form oxides other than silica behave differently under hydrothermal conditions. AlN forms AlOOH (95). Other ceramics such as ~~TiC~~ and ZrC which do not form protective oxides at high temperatures also do not form protective oxides under hydrothermal conditions (91).

VI. Liquid Metals

Ceramics have long been used as containers for processing of liquid metals. More recent applications involve use of liquid metals as a heat transfer medium. A wide range of non-oxide ceramics have been considered for these applications (12, 96, 97). Dissolution of the ceramic and capillary action are two important issues in liquid metal corrosion (12). Dissolution can be diffusion controlled or interface controlled. Local variations in dissolution due to phase and structural differences can lead to surface roughening. Capillary action leads to internal attack of porous ceramics. More important it can lead to substantial grain

boundary attack, depending on the relation of the solid/liquid interfacial energy and the grain boundary energy (12).

VII. Effect of Oxidation/Corrosion on Mechanical Properties

It is evident from current materials research that we cannot view one phenomenon such as oxidation or corrosion alone, but rather must view its effect on the entire system. Nearly all the applications listed in Table I utilize the ceramic in some type of load-bearing situation. A critical question that arises, is how oxidation and corrosion alter the ability of the ceramic to bear a load (98-112). Again, the emphasis here is on SiC and Si_3N_4 .

Two recent reviews summarize the critical issues involved in corrosion/mechanical property interactions (98, 99). Many of the studies in this area deal with the change in mechanical properties after corrosion. However these processes often act together. The oxidation rate for various types of Si_3N_4 is increased by the application of either compressive or tensile stresses (100,101).

It is well established that short-term oxidation tends to blunt cracks and may actually increase strength (103). Long-term isothermal oxidation (5000 h) for SiC containing B, C, and Si leads to strength increases whereas the same treatment for SiC containing Al₂O₃ and WC leads to strength decreases (104). Little strength degradation of a variety of commercial SiC and Si₃N₄ materials was observed for 3500h burner rig tests with 12 min. cycles (105). Recent research (106) shows the effects of water vapor on strength are complex, however, in some cases the rapid oxidation rates lead to flaw healing. In the case of stress rupture for Si₃N₄, water vapor has little effect (107).

Molten salt corrosion (108-110) leads to extensive pitting and strength reduction. Figure 20 is a fracture origin due to a corrosion pit from molten salt attack (108). This indicates the need for tougher, more flaw resistant ceramics. In the case of Si₃N₄ it has been shown that corrosion reactions often effect the grain boundary phase. Various mechanical properties are often related to the stability of this phase. Compositional changes in this grain boundary phase may lower the threshold stress intensity for crack growth and also increase the creep rate.

Corrosion reactions at a growing crack tip are quite important as evidenced by moisture-assisted crack growth of ceramics (111). Henager and Jones (112) have shown that the presence of Na₂SO₄ increases the slow crack growth velocity by a factor of two over air at 1573 K.

Similar effects occur in the case of hydrothermal corrosion. Pitting and dislodging of grains in various types of Si_3N_4 leads to substantial strength reductions. Analogous to the high temperature situation, changes in the grain boundary phase of Si_3N_4 lead to changes in the mechanical behavior. Weakening and dissolution of this phase leads to substantial strength reductions. Similarly, liquid metal attack of grain boundaries will lead to strength reductions (96).

VIII. Conclusions

Non-oxide ceramics are a promising class of materials for a wide range of applications at high temperatures. Before application, their interactions with the high temperature environment must be well-understood. The silica forming ceramics (SiC and Si_3N_4) exhibit the best oxidation behavior and the focus of this chapter is on them. However some information is included on AlN and BN which show promise for several specific applications.

High-temperature oxidation is critical to most applications. SiC oxidizes with the diffusion of oxygen inward through the growing silica scale being rate limiting.

The oxidation of Si_3N_4 is more complex—here the oxynitride scale plays a role.

Most engineering ceramics contain additives, which tend to enhance oxidation.

Actual applications involve complex gas mixtures. The effects of water vapor, carbon dioxide, low oxidant pressures, and mixed oxidizing/reducing gases are discussed. Water vapor enhances oxidation, whereas carbon dioxide is a less effective oxidant. Low oxidant pressures and mixed oxidizing/reducing gases lead to SiO(g) formation.

Corrosive deposits are also encountered in some applications. These include sodium sulfates, vanadate, and slags. Deposit-induced corrosion can be described with the acid/base theory of oxides. Since silica is an acidic oxide, it is readily attacked by a basic molten salt.

These problems may be minimized with the application of a refractory oxide coating. Mullite shows a good thermal expansion match to SiC and is a promising starting point. It may be possible to develop other more refractory oxide coatings.

The oxidation of Si_3N_4 is more complex—here the oxynitride scale plays a role.

Most engineering ceramics contain additives, which tend to enhance oxidation.

Actual applications involve complex gas mixtures. The effects of water vapor, carbon dioxide, low oxidant pressures, and mixed oxidizing/reducing gases are discussed. Water vapor enhances oxidation, whereas carbon dioxide is a less effective oxidant. Low oxidant pressures and mixed oxidizing/reducing gases lead to SiO(g) formation.

Corrosive deposits are also encountered in some applications. These include sodium sulfates, vanadate, and slags. Deposit-induced corrosion can be described with the acid/base theory of oxides. Since silica is an acidic oxide, it is readily attacked by a basic molten salt.

These problems may be minimized with the application of a refractory oxide coating. Mullite shows a good thermal expansion match to SiC and is a promising starting point. It may be possible to develop other more refractory oxide coatings.

Some proposed applications involve hydrothermal conditions—water at high temperatures and pressures. Hydrothermal corrosion is analogous to high temperature oxidation in many ways. Ceramics which form protective high temperature oxides also form protective hydrothermal oxides. The form of corrosive attack is also similar.

Finally the interaction of corrosive attack and degradation of ceramic properties is briefly discussed. This is essential to understand before these materials can be applied. Microstructural changes such as pitting and grain boundary attack lead to a concurrent loss of mechanical integrity. The development of tougher ceramics and coatings are necessary to minimize this problem.

Application	Non-Oxide Ceramic	Approximate Use Temperatures (°C)	Environment	References
Turbine engine components Combuster liners Blades & Vanes	SiC, Si ₃ N ₄ Composites	900-1400	Combustion gases, Deposits: Na, Mg, Ca sulfate, sodium vanadates	1
Piston engine components Pistons Valves	SiC, Si ₃ N ₄ Composites	900-1400	Combustion gases	2
Industrial Furnaces Heat Exchangers	SiC Composites	900-1400	Combustion gases, various deposits	3
Coal Combustion Particulate filters	SiC Composites	700-1000	Combustion gases, slag deposits	4
Chemical Process Vessels, Coal Gasifiers, Waste Incinerators	SiC, Si ₃ N ₄	900-1400	Various gases including air, H ₂ S, HCl	5
Re-entry Shields	SiC Composites	1000-1500	Reduced pressure N ₂ , O ₂ , CO ₂ , N ₂ O	6,7
High Temperature Semi-conductors	SiC	Use: 600 Processing: 1200	Air	8
Electronic Substrates	AlN	Use: 200 Processing: 1000	Air	9
Fiber Coatings for Composites, Crucibles, Insulators	BN	900-1400	Fiber coatings: reduced pressure combustion Crucibles: Vacuum, inert gases	10 11
Liquid metal containers	Various carbides	600-1400	Vacuum or inert gas and	12

Processing Heat transfer	and nitrides		liquid metals	
Pump bearings, Cooling lines for nuclear reactors	SiC, Si ₃ N ₄	300-600	High Pressure Fluids, 10 - 100 atm	13

Table I. Selected applications which are proposed for non-oxide ceramics.

Material	CTE (10^6 K^{-1})
SiC	5.2
Si_3N_4	3.2
Mullite ($3\text{Al}_2\text{O}_3 \cdot 2\text{SiO}_2$)	5.4
Alumina (Al_2O_3)	9
Partially stabilized zirconia ($0.08 \text{ Y}_2\text{O}_3 \cdot \text{ZrO}_2$)	10

Table II. Coefficients of thermal expansion of SiC and several refractory oxides (89).

References

1. HB Probst. Structural ceramics in heat engines—The NASA viewpoint. Proceedings of International Symposium on Ceramic Components for Heat Engines, Japan, 1983, pp 45-58.
2. AF McLean. Materials approach to engine/component design. Proceedings of the Second International Symposium on Ceramic Materials and Components for Engines, Bad Honnef, Germany, 1986, pp 1023-1034.
3. JI Federer, TN Tiegs, DM Kotnick, D Petrak. Analysis of candidate silicon carbide recuperator material exposed to industrial furnace environments. Rept. No. ORNL/TM-9677, Oak Ridge National Laboratory, 1985.
4. MK Ferber, J Ogle, VJ Tennery, T Henson. Characterization of corrosion mechanisms occurring in a sintered SiC exposed to basic coal slags. *J Am Ceram Soc* 68:191-197, 1985.
5. FA Costa Oliviera, RAH Edwards, RJ Fordham, JHW De Wit. Factors limiting the application of silicon nitride ceramics in sulphur-containing environments of low oxygen potential at high temperatures. In: KG Nickel, ed. *Corrosion of Advanced Ceramics Measurement and Modelling*. Dordrecht, The Netherlands: Kluwer, 1994, pp 177-188.

6. A Lacombe, C. Bonnet. Ceramic matrix composites, key materials for future space plane technologies. Proceedings of the AIAA Second International Aerospace Planes Conference, Orlando, FL, 1990.
7. NS Jacobson, RA Rapp. Thermochemical degradation mechanisms for the reinforced carbon/carbon panels on the space shuttle. NASA Technical Memorandum 106793, 1995.
8. VE Chelnokov, AL Syrkin. High temperature electronics using SiC: actual situation and unsolved problems. Mat Sci Eng B46:248-253, 1997.
9. PA Janeway. Aluminum Nitride: Making the grade in demanding electronic applications. Ceram Ind, July 1991.
10. CH Henager Jr., RH Jones. Effects of an aggressive environment on the subcritical crack growth of a continuous-fiber ceramic matrix composite. Ceram Eng Sci Proceedings 13:411-419, 1992.
11. A Lepp, KA Schwetz, K Hunold. Hexagonal boron nitride: Fabrication, properties, and applications. J Eur Ceram Soc 5:3-9, 1989.

12. R Sangiorgi. Corrosion of ceramics by liquid metals. In: KG Nickel, ed. *Corrosion of Advanced Ceramics Measurement and Modelling*. Dordrecht, The Netherlands: Kluwer, 1994, pp 261-284.
13. K Oda, T Yoshio, Y Miyamoto, M Koizumi. Hydrothermal corrosion of pure, hot isostatically pressed silicon nitride. *J Am Ceram Soc* 76:1365-1368, 1993.
14. NJ Shaw, JA DiCarlo, NS Jacobson, SR Levine, JA Nesbitt, HB Probst, WA Sanders, CA Stearns. Materials for engine applications above 3000 °F—an overview. *NASA Technical Memorandum* 100169, 1987.
15. MA Lamkin, FI Riley, RJ Fordham. Oxygen mobility in silicon dioxide and silicate glasses: a review. *J Eur Ceram Soc* 10:347-367, 1992.
16. FJ Norton. Permeation of gaseous oxygen through vitreous silica. *Nature* 171:701, 1961.
17. EJ Opila. Influence of alumina reaction tube impurities on the oxidation of chemically-vapor-deposited silicon carbide. *J Am Ceram Soc* 78:1107-1110, 1995.
18. BE Deal, AS Grove. General relationship for the thermal oxidation of silicon. *J Appl Phys* 36:3770-3778, 1965.

19. JA Costello, RE Tressler. Oxidation kinetics of silicon carbide crystals and ceramics: I, In dry oxygen. *J Am Ceram Soc* 69:674-681, 1986.
20. LUJT Ogbuji, EJ Opila. A comparison of the oxidation kinetics of SiC and Si_3N_4 . *J Electrochem Soc* 142:925-930, 1995.
21. CE Ramberg, G Cruciani, KE Spear, RE Tressler, CF Ramberg Jr. Passive-oxidation kinetics of high-purity silicon carbide from 800 to 1100°C. *J Am Ceram Soc* 79:2897-2911, 1996.
22. K Motzfeldt. On the rates of oxidation of silicon and silicon carbide in oxygen, and correlation with permeability of silica glass. *Acta Chem Scand* 18:1596-1606, 1964.
23. Z Zheng, RE Tressler, KE Spear. Oxidation of single-crystal silicon carbide, Part II. Kinetic model. *J Electrochem Soc* 137:2812-2816, 1990.
24. NS Jacobson. Corrosion of silicon-based ceramics in combustion environments. *J Am Ceram Soc* 76:3-28, 1993.
25. KL Luthra. Some new perspectives on oxidation of silicon carbide and silicon nitride. *J Am Ceram Soc* 74:1095-1103, 1991.

26. Z Zheng, RE Tressler, KE Spear. Oxidation of single-crystal silicon carbide, Part I. Experimental studies. *J Electrochem Soc* 137:854-858, 1990.
27. WC Tripp, JW Hinze, MG Mendiratta, RH Huff, AF Hampton, JE Stroud, ET Rodine. Internal structure and physical properties of ceramics at high temperatures. *Aerospace Research Laboratories report #75-0130*, 1975, pp 116-125
28. CE Ramberg. PhD dissertation, University of Pennsylvania, Philadelphia, PA, 1997.
29. LUJT Ogbuji. Effect of oxide devitrification on oxidation kinetics of SiC. *J Am Ceram Soc* 80:1544-1550, 1997.
30. LUJT Ogbuji, DT Jayne. Mechanism of incipient oxidation of bulk chemical vapor deposited Si_3N_4 . *J Electrochem Soc* 140:759-766, 1993.
31. LUJT Ogbuji, SR Bryan. The SiO_2 - Si_3N_4 interface, Part I: Nature of the interphase. *J Am Ceram Soc* 78:1272-1278, 1995.
32. BW Sheldon. Silicon nitride oxidation based on oxynitride interlayers with graded stoichiometry. *J Am Ceram Soc* 79:2993-2996, 1996.

33. H Du, RE Tressler, KE Spear, CG Pantano. Oxidation studies of crystalline CVD silicon nitride. *J Electrochem Soc* 136:1527-1536, 1989.
34. D Cubicciotti, KH Lau. Kinetics of oxidation of hot-pressed silicon nitride containing magnesia. *J Am Ceram Soc* 61:512-517, 1978.
35. D Cubicciotti, KH Lau. Kinetics of oxidation of yttria hot-pressed silicon nitride. *J Electrochem Soc* 126:1723-1728, 1979.
36. JA Costello, RE Tressler, IST Tong. Boron redistribution in sintered α -SiC during thermal oxidation. *J Am Ceram Soc* 64:332-335, 1981.
37. DM Mieskowski, WA Sanders. Oxidation of silicon nitride sintered with rare-earth oxide additions. *J Am Ceram Soc* 68:C160-C163, 1985.
38. P Andrews, FL Riley. The microstructure and composition of oxide films formed during high-temperature oxidation of a sintered Si_3N_4 . *J Eur Ceram Soc* 5:245-256, 1989.
39. SC Singhal, FF Lange. Effect of alumina content on the oxidation of hot-pressed silicon carbide. *J Am Ceram Soc* 58:433-435, 1975.

40. DS Fox. Oxidation behavior of chemically vapor-deposited silicon carbide and silicon nitride from 1200-1600°C. Accepted for publication J Am Ceram Soc.
41. M Backhaus-Ricault, YG Gogotsi. Identification of oxidation mechanisms in silicon nitride ceramics by transmission electron microscopy studies of oxide scales. J Mater Res 10:2306-2321, 1995.
42. P Andrews, FL Riley. Silicon nitride oxidation/reoxidation. J Eur Ceram Soc. 7:125-132, 1991.
43. J Persson, P-O Kall, M Nygren. Parabolic non-parabolic oxidation kinetics of Si_3N_4 . J Eur Ceram Soc 12:177-184, 1993.
44. JK Patel, DP Thompson. The low-temperature oxidation problem in yttria-densified silicon nitride ceramics. Br Ceram Trans J 87:70-73, 1988.
45. RB Sosman. The Properties of Silica. New York: The Chemical Catalog Company, Inc., 1927, p364.
46. EJ Opila, DS Fox, CA Barrett. Cyclic oxidation of monolithic SiC and Si_3N_4 materials. Cer Eng Sci Proc 14 [7-8]: 367-374.

47. NS Jacobson, S Farmer, A Moore, H Sayir. High temperature oxidation of boron nitride Part I—Monolithic boron nitride. submitted to J. Am. Ceram. Soc.
48. K Vedula, W Williams, AH Heuer, TE Mitchell, F Lisy, A Abada, DC Wang. Ultra high-temperature ceramic-ceramic composites. Proceedings of Ultra-High Temperature Composite Materials Meeting, Dayton, OH, 1988.
49. A Bellosi, E Landi, A Tampieri. Oxidation behavior of aluminum nitride. *J Mater Res* 8:565-572, 1993.
50. D Robinson, R Dieckmann. Oxidation of aluminum nitride substrates. *J Mat Sci* 29:1949-1957, 1994.
51. T Sato, K Haryu, T Endo, M Shimada. High temperature oxidation of hot-pressed aluminum nitride by water vapor. *J Mat Sci* 22:2270-2280, 1987.
52. DA Robinson, G Yin, R Dieckmann. Oxide film formation on aluminum nitride substrates covered with thin aluminum layers. *J Mat Sci* 29:2389-2394, 1994.
53. H Kim, AJ Moorhead. Oxidation behavior and flexural strength of aluminum nitride exposed to air at elevated temperatures. *J Am Ceram Soc* 77:1037-1041, 1994.

54. EJ Opila. The variation of the oxidation rate of SiC with water vapor pressure.

Submitted to J Am Ceram Soc

55. EJ Opila. Oxidation kinetics of chemically vapor-deposited silicon carbide in wet oxygen. *J Am Ceram Soc* 77:730-736, 1994.

56. V Pareek, DA Shores. Oxidation of silicon carbide in environments containing potassium salt vapors. *J Am Ceram Soc* 74:556-63, 1991.

57. RE Tressler, JA Costello, Z Zheng. Oxidation of silicon carbide ceramics. In: AJ Hayes, ed. *Industrial Heat Exchangers*. Warrendale, PA: American Society of Metals, 1985, pp 307-314.

58. DJ Choi, DB Fischbach, WD Scott. Oxidation of chemically-vapor-deposited silicon nitride and single crystal silicon. *J Am Ceram Soc* 72:1118-1123, 1989.

59. JE Antill, JB Warburton. Oxidation of silicon and silicon carbide in gaseous atmospheres at 1000°-1300°C. In: *Reactions between Solids and Gases*, AGARD CP-52. Paris: Advisory Group for Aerospace Research and Development, 1970, pp 10-1 to 10-14.

60. G Hetherington, KH Jack, JC Kennedy. The viscosity of vitreous silica. Phys Chem Glasses 5:130-136, 1964.
61. A Hashimoto. The effect of H₂O gas on volatilities of planet-forming major elements: I. Experimental determination of thermodynamic properties of Ca-, Al-, and Si-hydroxide gas molecules and its application to the solar nebula. Geochim Cosmochim Acta 56:511-532, 1992.
62. EJ Opila, DS Fox, NS Jacobson. Mass spectrometric identification of Si-O-H(g) species from the reaction of silica with water vapor at atmospheric pressure. J Am Ceram Soc 80:1009-1012 (1997).
63. EJ Opila, RE Hann Jr. Paralinear oxidation of CVD SiC in water vapor. J Am Ceram Soc 80:197-205, 1997.
64. AC Lea. The oxidation of silicon-carbide refractory materials. J Soc Glass Tech 33: 27-50, 1949.
65. E Fitzer, R Ebi. Kinetic studies on the oxidation of silicon carbide. In: RC Marshall, JW Faust Jr., CE Ryan, ed. Silicon Carbide 1973. Columbia, South Carolina: University of South Carolina Press, 1974, pp 320-328.

66. W Bremen, A Naoumidis, H Nickel. Oxidation behavior of pyrolytically deposited β -SiC in an atmosphere composed of CO-CO₂ gas mixtures. *J Nucl Mater* 71: 56-64, 1977.
67. EJ Opila, QN Nguyen. The oxidation of silicon carbide in carbon dioxide. In preparation for *J Am Ceram Soc*.
68. EJ Opila, NS Jacobson. SiO(g) formation from SiC in mixed oxidizing-reducing gases. *Oxid Met* 44:527-544, 1995.
69. DP Butt, RE Tressler, KE Spear. Durability of SiC materials in gaseous N₂-H₂-CO heat treat environments I. *Ind Heat* 58:44-48, 1991.
70. C Wagner. Passivity during the oxidation of silicon at elevated temperatures. *J Appl Phys* 29:1295-1298, 1958.
71. SC Singhal. Thermodynamic analysis of the high-temperature stability of silicon nitride and silicon carbide. *Ceram Int* 2:123-130, 1976.
72. HE Kim, DW Readey. Active oxidation of SiC in low dew-point hydrogen above 1400°C. *Proceedings of Silicon Carbide '87*, Columbus, OH, 1989, pp 301-312.

73. T Narushima, T Goto, Y Yokoyama, Y Iguchi, T Hirai. High-temperature active oxidation of chemically vapor-deposited silicon carbide in CO-CO₂ atmosphere. *J Am Ceram Soc* 76:2521-2524, 1993.
74. T Narushima, T Goto, Y Iguchi, T Hirai. High-Temperature active oxidation of chemically vapor-deposited silicon carbide in an Ar-O₂ Atmosphere. *J Am Ceram Soc* 74:2583-2586, 1991.
75. JE Marra, ER Kreidler, NS Jacobson, DS Fox. Reactions of silicon-based ceramics in mixed oxidation chlorination environments. *J Am Ceram Soc* 71:1067-1073, 1988.
76. P Steinmetz, C Rapin. La corrosion des materiaux dans les incinérateurs de déchets ménagers. To appear in Proceedings of the 4th International Symposium on High Temperature Corrosion and Protection of Materials, Les Embiez, France, 1996.
77. Z Zheng, RE Tressler, KE Spear. The effect of sodium contamination on the oxidation of single-crystal silicon carbide. *Corros Sci* 33:545-566, 1992.
78. Z Zheng, RE Tressler, KE Spear. A comparison of the oxidation of sodium-implanted CVD Si₃N₄ with the oxidation of sodium-implanted SiC-crystals. *Corros Sci* 33:569-580, 1992.

79. FS Pettit, CS Giggins. Hot corrosion. In: CT Sims, NS Stoloff, and WC Hagel, ed. Superalloys II. New York: Wiley, 1990, pp 327-354.
80. NS Jacobson, JL Smialek, DS Fox. Molten salt corrosion of SiC and Si_3N_4 . In: NP Cheremisinoff, ed. Handbook of Ceramics and Composites, Vol 1, Synthesis and Properties. New York: Marcel Dekker, 1990, pp 99-136.
81. NS Jacobson. Sodium sulfate: Deposition and dissolution of silica. *Oxid Met* 31:91-103, 1989.
82. CA Stearns, FJ Kohl, DE Rosner. Combustion system processes leading to corrosive deposits. Proceedings of High Temperature Corrosion, NACE, San Diego, 1981, pp 441-450.
83. DS Fox, MD Cuy, TE Strangman. Sea salt hot corrosion and strength of a yttria-containing silicon nitride. *J Am Ceram Soc* in press.
84. Y. Dessureault, J Sangster, AD Pelton. Coupled phase diagram/thermodynamic analysis of the nine common-ion binary system involving the carbonates and sulfates of lithium, sodium, and potassium. *J Electrochem Soc* 137:2941-2950, 1990.

85. MA Lamkin, FL Riley, RJ Fordham. Hot corrosion of silicon nitride in the presence of sodium and vanadium compounds. Proceedings of High Temperature Corrosion of Technical Ceramics, London, 1990, pp 181-191.
86. PF Becher. Strength degradation in SiC and Si_3N_4 ceramics by exposure to coal slags at high temperatures. J Mat Sci 19:2805-2814, 1984.
87. NS Jacobson, KN Lee, DS Fox. Reactions of silicon carbide and silicon (IV) oxide at elevated temperatures. J Am Ceram Soc 75:1603-1611, 1992.
88. KN Lee, RA Miller, NS Jacobson. New generation of plasma-sprayed mullite coatings on silicon carbide. J Am Ceram Soc 78:705-710, 1995.
89. KN Lee, NS Jacobson, RA Miller. Refractory oxide coatings on SiC ceramics. MRS Bulletin XIX:35-38, 1994.
90. N Boukis, N Claussen, K Ebert, R. Janssen. Corrosion screening tests of high-performance ceramics in supercritical water containing oxygen and hydrochloric acid. J Eur Ceram Soc 17:71-76, 1997.
91. M Yoshimura, JI Kase, M Hayakawa, S Somiya. Oxidation mechanism of nitride and carbide powders by high-temperature, high-pressure water. Ceram Trans 10:337-354, 1990.

92. NS Jacobson, YG Gogotsi, M Yoshimura. Thermodynamics and experimental study of carbon formation on carbides under hydrothermal conditions. *J Mater Chem* 5:595-601, 1995.
93. YG Gogotsi, M Yoshimura. Formation of carbon films on carbides under hydrothermal conditions. *Nature* 367:628-630, 1994.
94. T Yoshio, K Oda. Aqueous corrosion and pit formation of Si_3N_4 under hydrothermal conditions. *Ceram Trans* 10:367-386, 1990.
95. T Yoshio, K. Oda. Durability of AlN ceramics in aqueous environment. *Proceedings of the Annual Meeting of the Ceramic Society of Japan*, 1995, pp 223-228.
96. JW Cree, MF Amateau. Degradation of silicon carbide by molten lithium. *J Am Ceram Soc* 70:C318-C319, 1987.
97. U Schwabe, LR Wolff, FJJ van Loo, G Ziegler. Corrosion of technical ceramics by molten aluminum. *J Eur Ceram Soc* 9:407-415, 1992.
98. RE Tressler. Environmental effects on the long-term reliability of SiC and Si_3N_4 ceramics. *Ceram Trans* 10:99-123, 1990.

99. KG Nickel, R Danzer, G Schneider, G Petzow. Corrosion and oxidation of advanced ceramics. Powder Metall Int 21:29-34, 1989.
100. GA Gogotsi, YG Gogotsi, VP Zavada, VV Traskovsky. Stress corrosion of silicon nitride based ceramics. Ceram Int 15:305-310, 1989.
101. YG Gogotsi, GG Grathwohl. Stress-enhanced oxidation of silicon nitride ceramics. J Am Ceram Soc 76:3093-3104, 1993.
102. TE Easler, RC Bradt, RE Tressler. Strength distributions of SiC ceramics after oxidation and oxidation under load. J Am Ceram Soc 64:731-734, 1981.
103. K Jakus, JE Ritter Jr, WP Rogers. Strength of hot-pressed silicon nitride after high temperature exposure. J Am Ceram Soc 67:472-475, 1984.
104. PF Becher. Strength retention in SiC ceramics after long-term oxidation. J Am Ceram Soc 66:C120-C121, 1983.
105. LJ Lindberg. Durability testing of ceramic materials for turbine engine applications. Proceedings of the Twenty Fourth Automotive Development Contractors' Coordination Meeting, Detroit, 1986, pp 79-86.

106. HS Rho, NL Hecht, GA Graves. The behavior of two Si_3N_4 and two SiC ceramics subject to oxidation environments. *Ceram Eng Sci Proc*, 1997, in press.
107. M Kaji, T Ono, M Higashi, A Kokaji. Stress rupture behavior a silicon nitride under combustion gas environment. *Proceedings Yokohama International Gas Turbine Congress*, 1995, pp 59-66.
108. JL Smialek, NS Jacobson. Mechanism of strength degradation for hot corrosion of α -SiC. *J Am Ceram Soc* 69:741-752, 1986.
109. JJ Swab, GL Leatherman. Strength of structural ceramics after exposure to sodium sulfate. *J Eur Ceram Soc* 5:333-340, 1989.
110. WJ Tomlinson, DM Caslin. Strength of SiC and SiC-7.4 vol% TiB_2 composite after corrosion with Na_2SO_4 and NaCl deposits. *Ceram Int* 17:61-66, 1991.
111. SM Wiederhorn. Moisture-assisted crack growth in ceramics. *Int J Fract Mech* 4:171-177, 1968.
112. CH Henager Jr, RH Jones. Molten salt corrosion of hot-pressed $\text{Si}_3\text{N}_4/\text{SiC}$ -reinforced composites and the effects of molten salt exposure on slow crack growth of hot-pressed Si_3N_4 . *Ceram Trans* 10:197-210, 1990.

Figure Captions

1. Equilibrium gas composition vs. equivalence ratio (24).
2. Recession due to oxidation for selected materials, with protective oxide scale indicated (14).
3. Structure of SiO₂ (a) Amorphous (b) Crystalline (c) With sodium cations (Adapted from (15))
4. Schematic of electro-balance and vertical tube furnace used for oxidation studies.
5. Oxidation of SiC at 1300 C in 1 atm oxygen, showing parabolic kinetics (20).
6. Arrhenius plot of log k_p vs 1/T for Si, CVD SiC, CVD Si₃N₄, and Si₃N₄ with additives obtained in dry oxygen(18, 20, 35).
7. Thermal expansion of SiC, Si₃N₄, amorphous SiO₂, and crystalline SiO₂ as a function of temperature (24).
8. Cyclic oxidation kinetics of SiC and Si₃N₄ (46).
9. Bubbles formed in SiO₂ due to oxidation of SiC in 90% water vapor/10% O₂ at 1200°C (54).
10. Schematic showing components of paralinear kinetics (63).
11. Comparison of SiC oxidation in 50% H₂O/O₂ , O₂, and CO₂ at 1200°C (67).
12. Calculated active/passive and passive/active transitions and measured active/passive transitions (72-74).
13. Schematic of jet fuel burner used for corrosion studies.

14. Optical micrographs of sintered SiC coupons with carbon and boron additives, oxidized in a burner rig at 1000°C (a) 46 h with no sodium (b) 13.5 h with sodium chloride seeded flame (24).
15. Calculated dew points for Na₂SO₄ deposition (81).
16. Quartz coupons treated in burner rig for 1 h with 2 ppm sodium (as NaCl) seeded flame: (a) No. 2 diesel fuel (0.5% sulfur), 5 h (b) Jet A fuel (0.05% sulfur) (81).
17. CVD SiC oxidized for 1 h at 1800°C (Courtesy of D. Fox, NASA Lewis).
- 18(a). Total pressure [P(SiO) + P(CO)] generated from SiC/SiO₂ interactions.
and (b). Total pressure [P(SiO) + P(N₂)] generated from Si₂N₂O/SiO₂ interactions (24).
19. Micrograph of polished cross-section of mullite on SiC (88).
20. Fracture origin for sintered α -SiC reacted with Na₂SO₄ for 48h at 1000°C (108). The area noted in (b) is enlarged in (c). (c) Preferential grain boundary attack is observed at arrows.

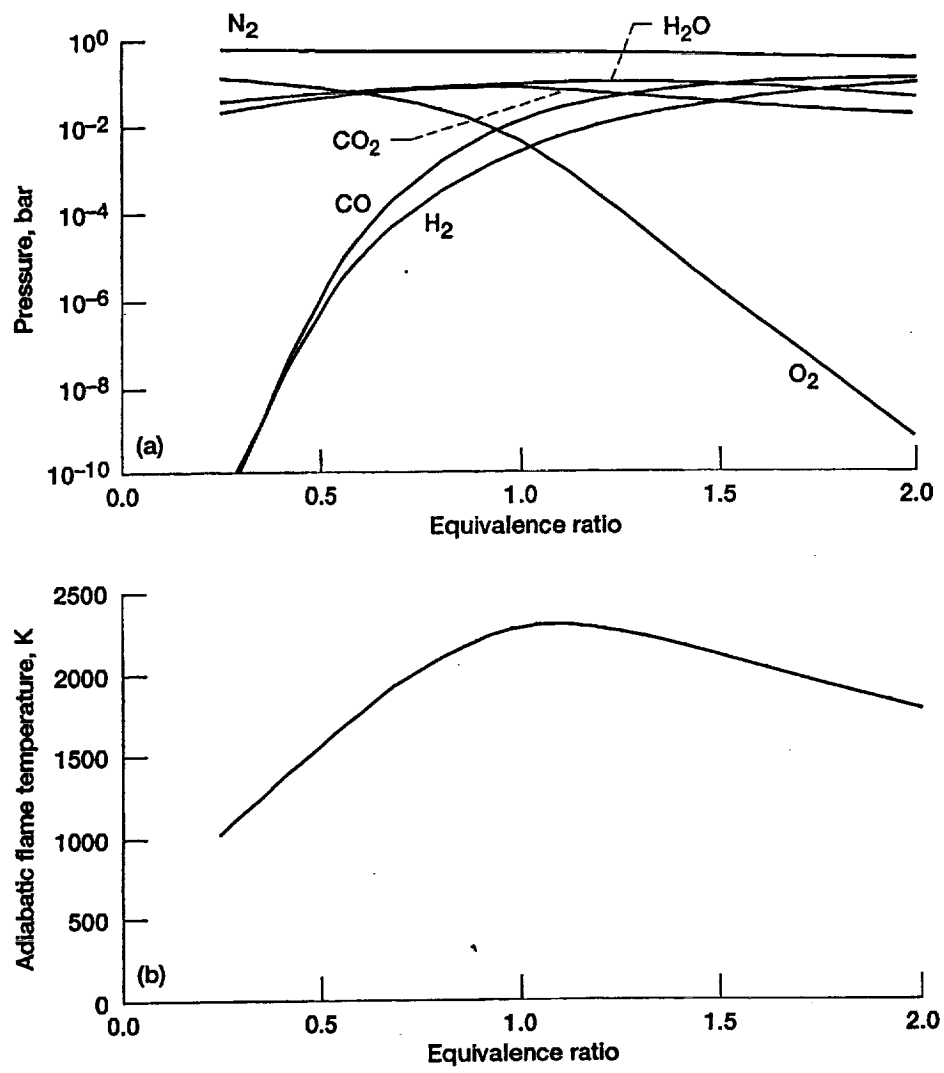


Figure 1.

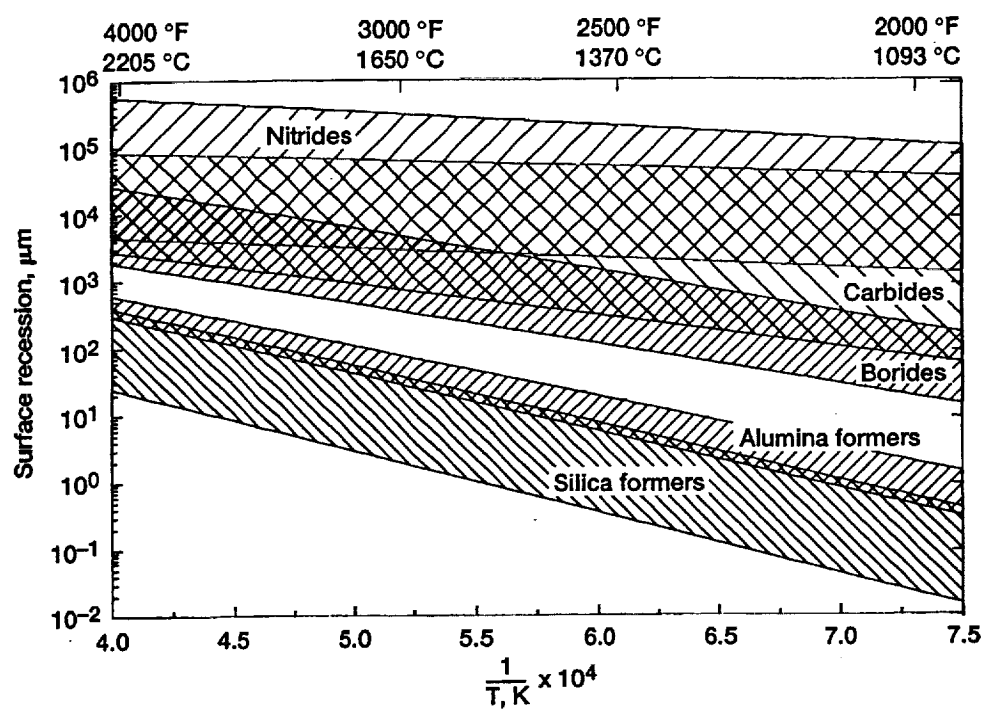


Figure 2.

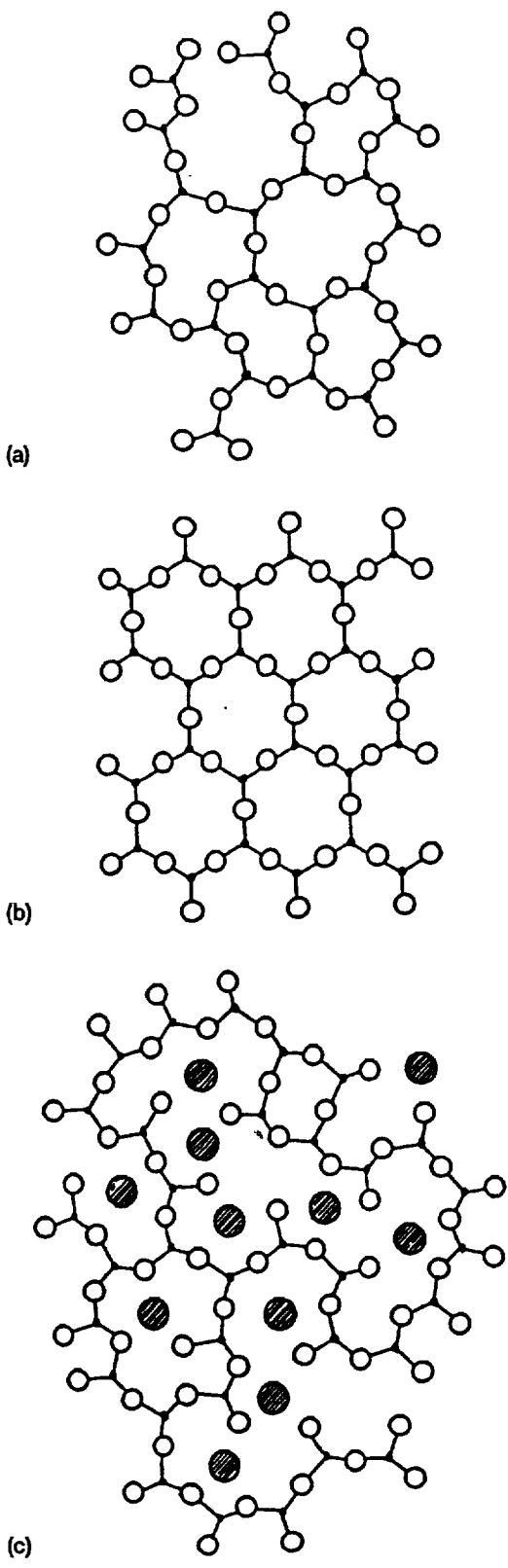


Figure 3.

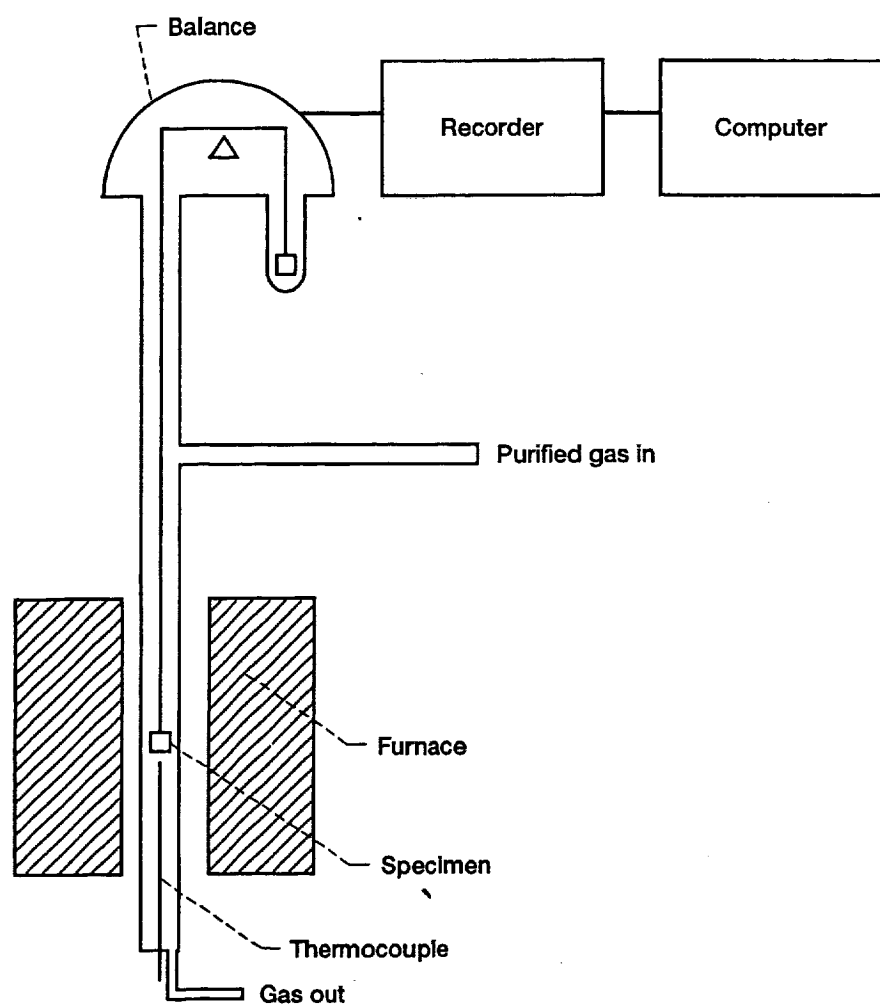


Figure 4.

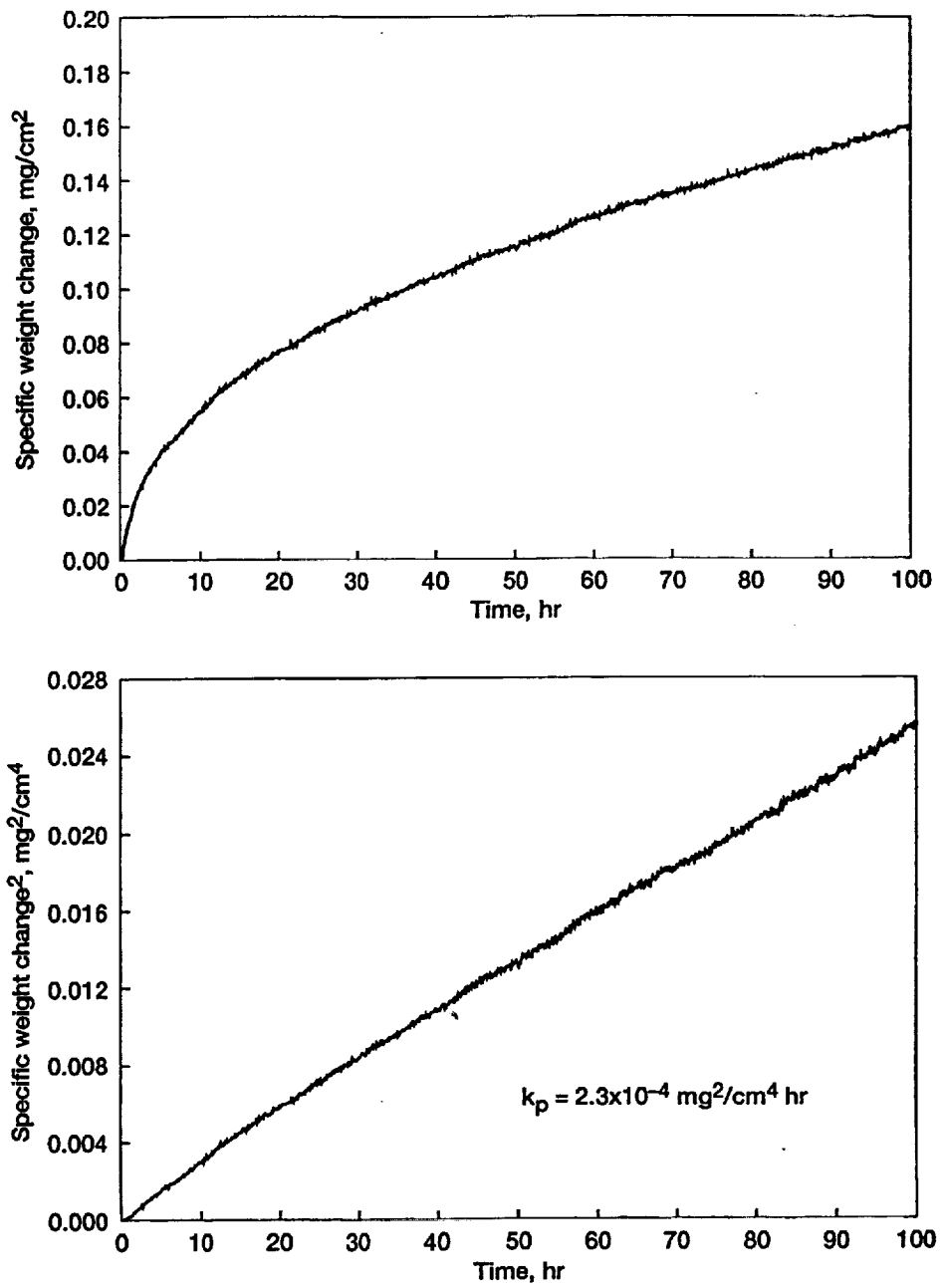


Figure 5.

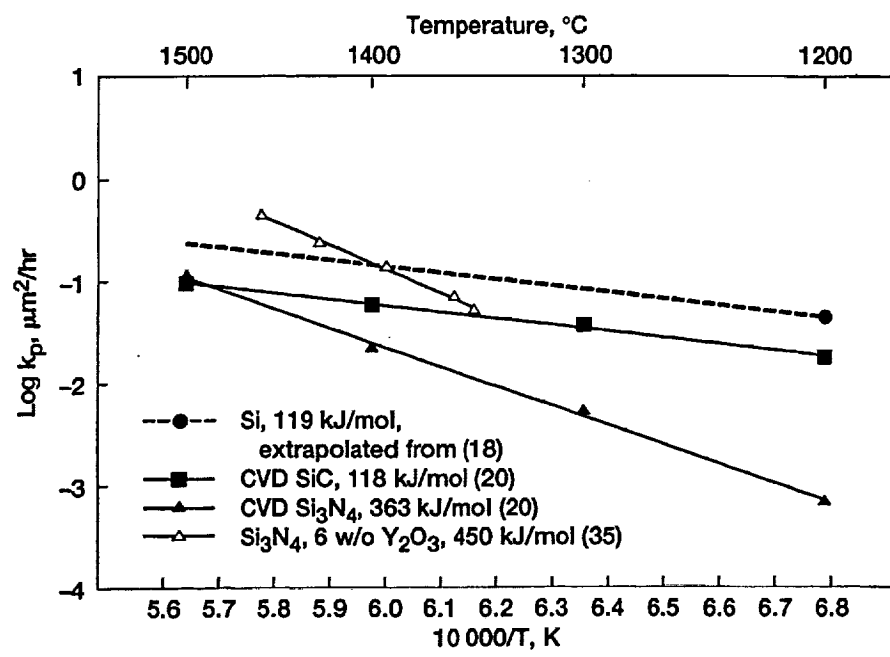


Figure 6.

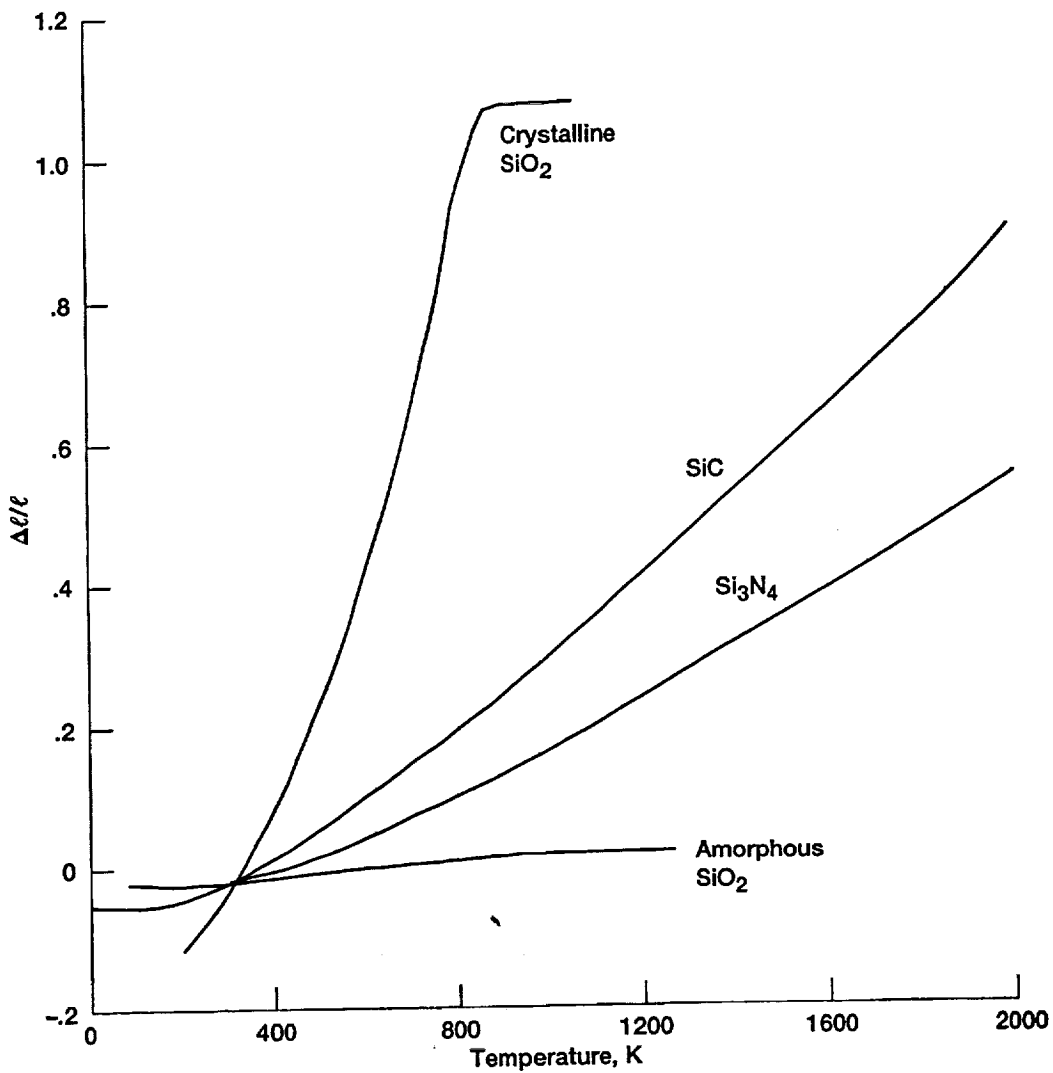


Figure 7.

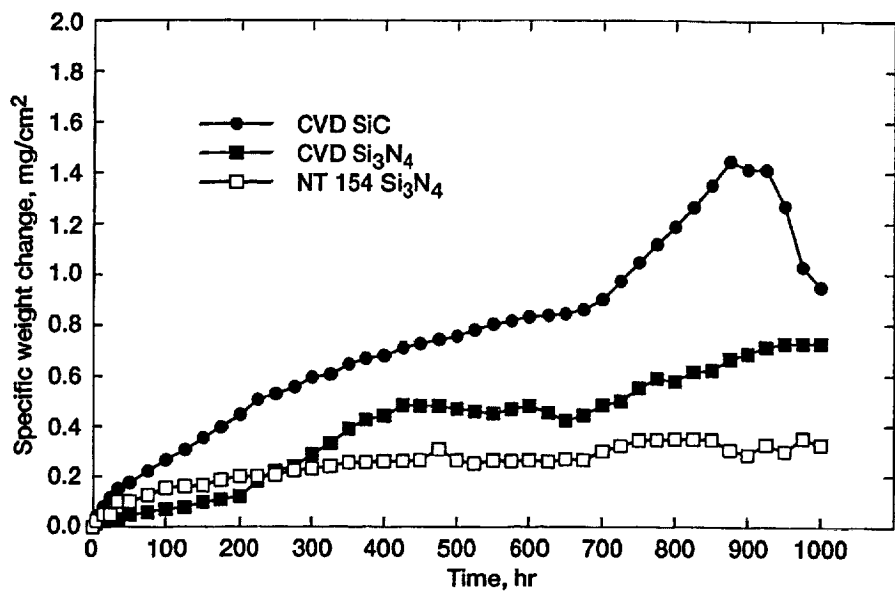


Figure 8.

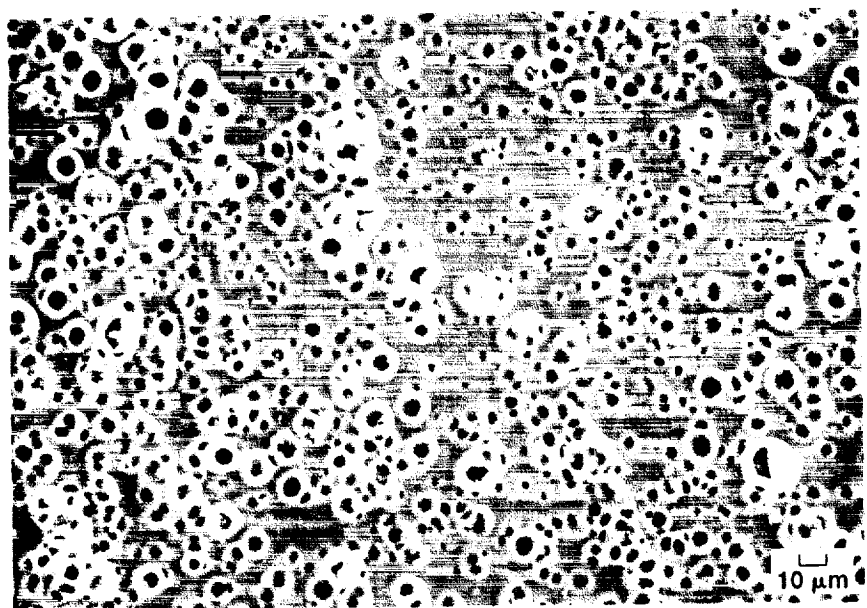


Figure 9.

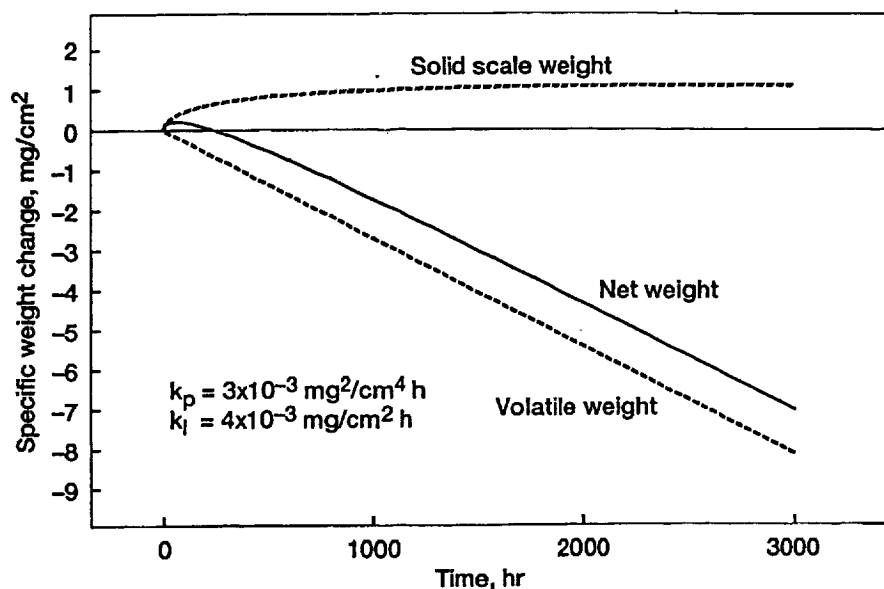


Figure 10.

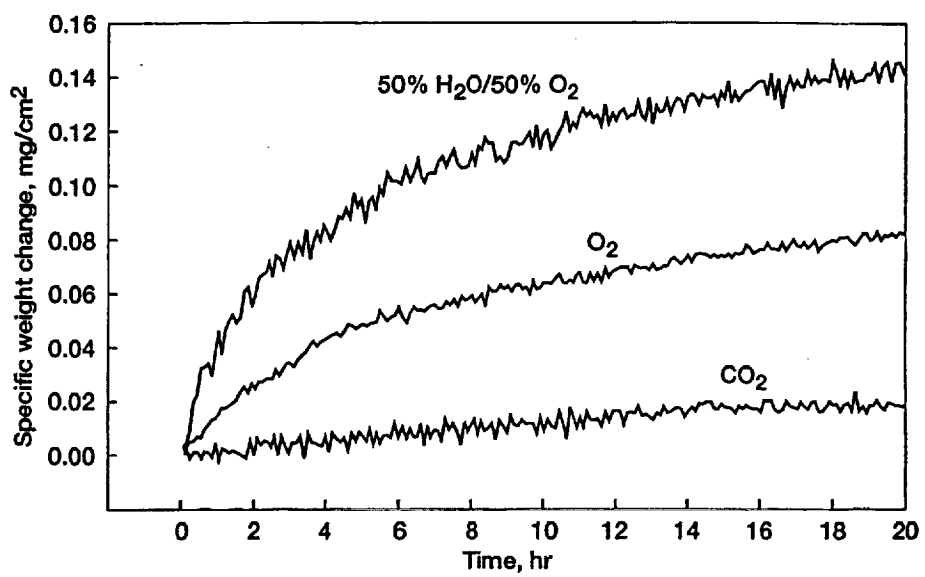


Figure 11.

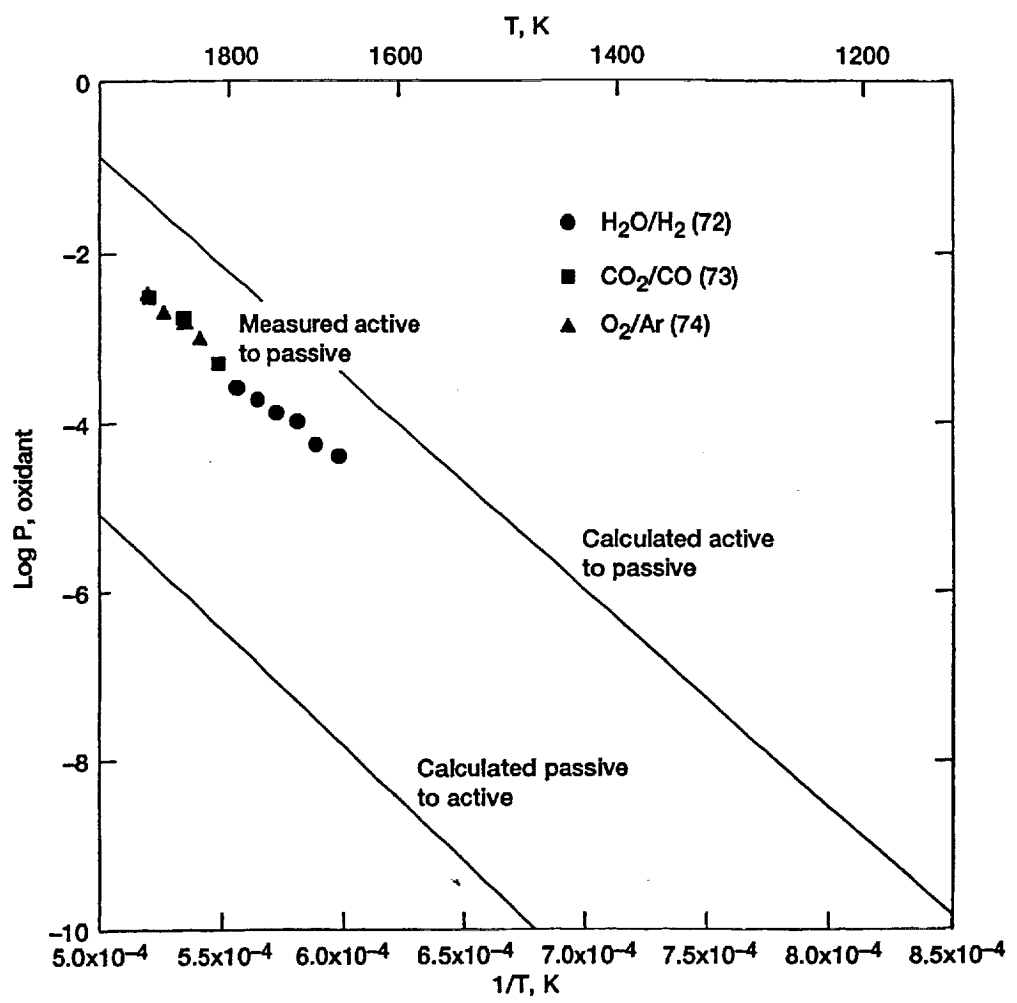


Figure 12.

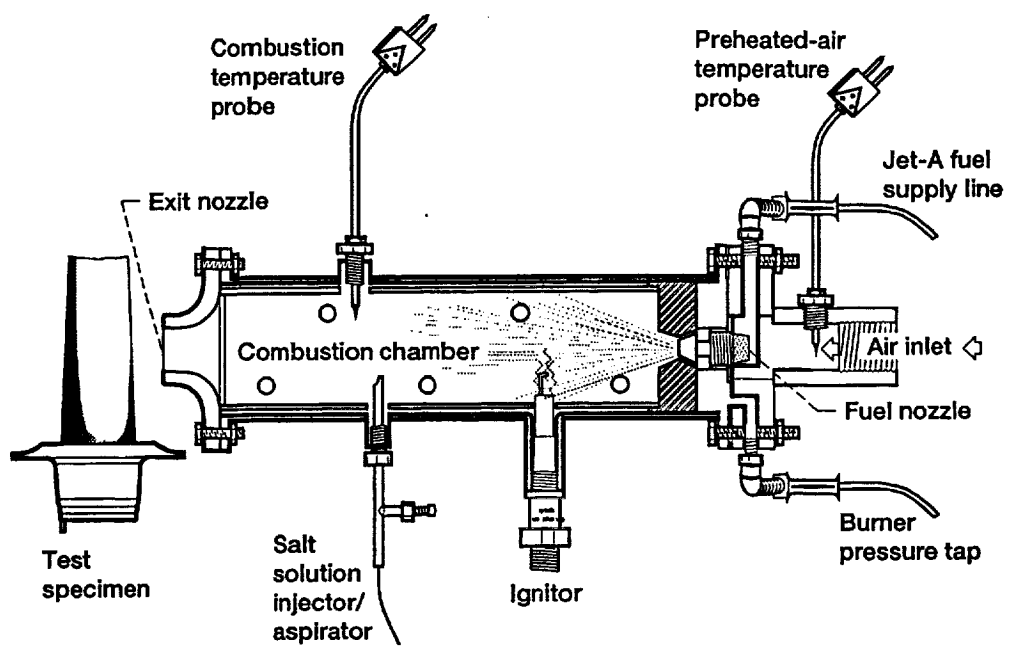


Figure 13.

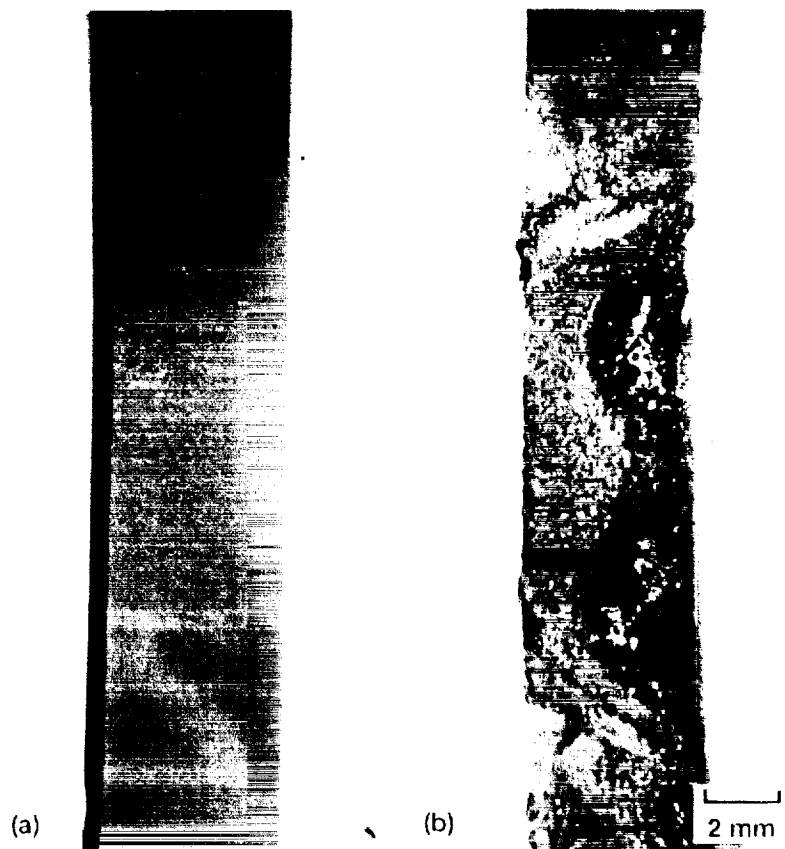


Figure 14.

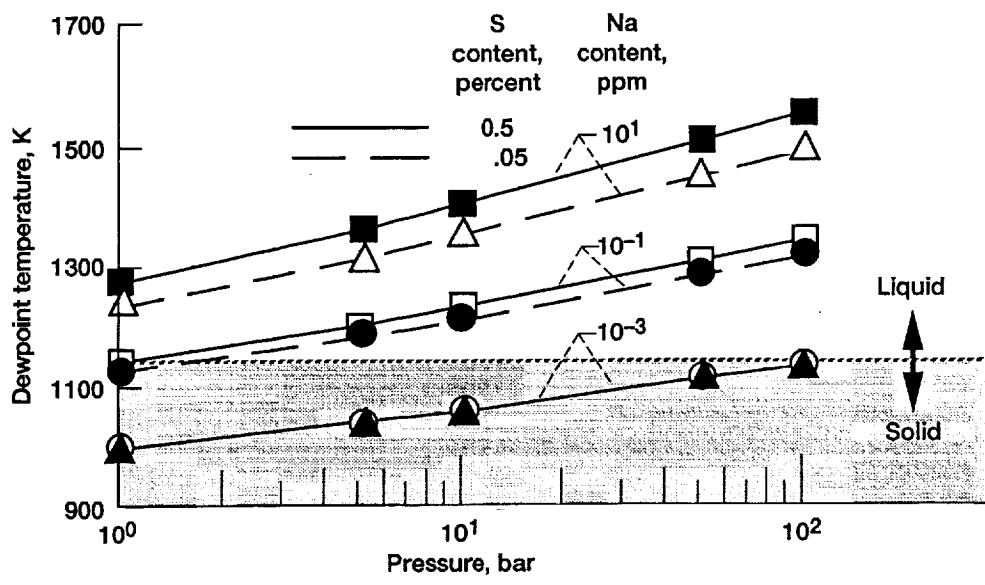


Figure 15.



Figure 16.



Figure 17.

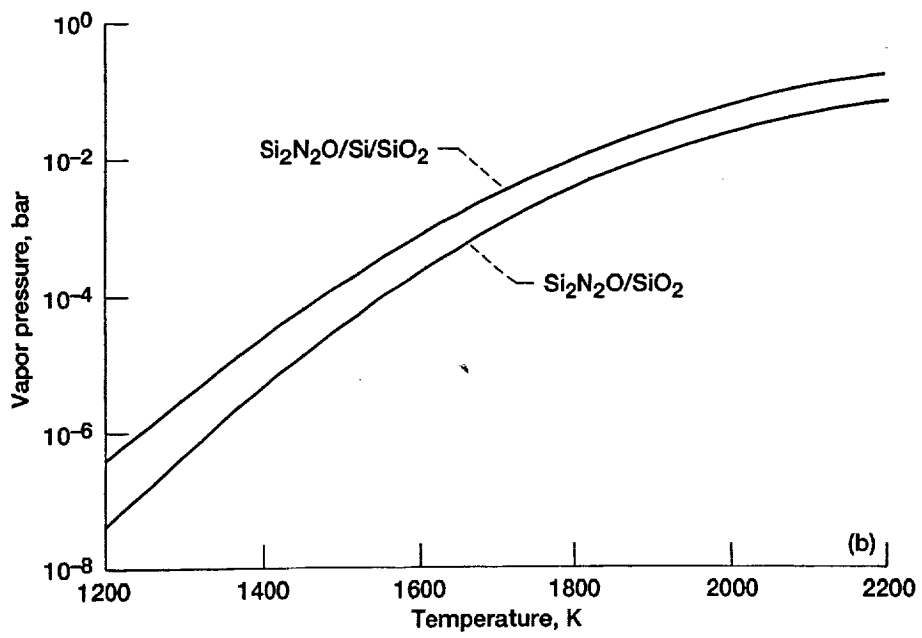
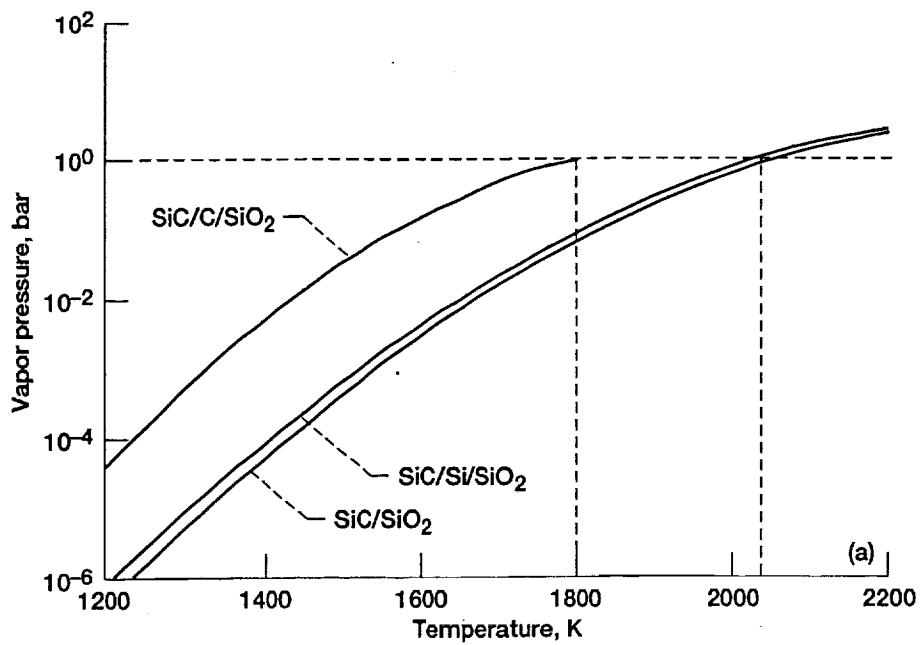


Figure 18.



Figure 19.



Figure 20.